Plasmonics (2020) 15:441–447
https://doi.org/10.1007/s11468-019-01046-0

Hybrid Dielectric-Plasmonic Nanocomposite Arrays for Bulk and Local Refractive Index Sensing

Praveenkumar Pinapati[1] · Sudhir Cherukulappurath[1]

Received: 8 August 2019 / Accepted: 30 September 2019 / Published online: 13 November 2019

Abstract

Plasmonics-based biosensors are often limited by material losses in the form of joule heating while all dielectric nanoparticles systems have relatively smaller local electric field enhancements. For efficient sensing, it is desirable to have a system with high sensitivity but with minimal losses. Here, we demonstrate, using numerical simulations, the capability of a hybrid dielectric-plasmonic system for refractive index sensing applications. We show that the optical resonances of such a hybrid system have smaller linewidths and the peak wavelengths are tunable. Bulk as well as local refractive index sensing are demonstrated in this work. Owing to large sensitivities of 300 nm/RIU with a figure of merit (FOM) of 10, the hybrid photonic-plasmonic systems presented here are promising materials for future biosensing applications.

Keywords Hybrid nanocomposites · Plasmonic sensing · Dielectric nanoparticle arrays

Introduction

Localized surface plasmon resonance (LSPR)-based biosensors have gained lot of interest owing to their large sensitivity to refractive index changes [1–3]. However, in order to achieve lower limits of detection, it is desirable to have not only large sensitivity toward change in the local refractive index but also narrow resonance linewidths. Plasmonic nanoparticles are susceptible to joule heating, especially in the visible frequencies of light, thereby broadening the resonances. Recently, there are reports on all-dielectric nanostructures as promising replacement for plasmonic systems due to their strong electric as well as magnetic scattering resonances at optical wavelengths [4–7]. Novel applications for metamaterials including negative refractive index and superlensing have been demonstrated using all dielectric nanostructures [8, 9]. The principle advantage of high-refractive index dielectric nanoparticles over plasmonic nanostructures is the absence of dissipative joule losses. This has led several researchers to investigate the properties of all-dielectric optical resonators in applications including biosensing devices [10–12]. Dielectric-based nanoresonators facilitate the manipulation of local electric as well as magnetic fields. Strong magnetic resonances, that are generally considered difficult to be excited in plasmonic nanostructures, can be observed in dielectric nanoresonators. Magnetic resonances are driven by the electric field of light that couples to the circular displacement current thereby inducing a magnetic dipole moment perpendicular to the electric field [13]. As in the case of plasmonic metals, resonances in dielectric sub-wavelength structures can be tuned by proper engineering of the geometry, the constitutive material properties, and the surrounding medium [14, 15]. Owing to these advantages, all-dielectric structures are being utilized in developing metamaterials and metasurfaces that can form as a platform for 2D optical devices. Subwavelength particles of silicon exhibiting multipolar electrical and magnetic resonances in the visible range of the electromagnetic spectrum have shown to be useful as biosensors. Recently, it was reported that all dielectric biosensing system based on silicon nanoparticle arrays can be used for the detection of small biomolecules such as streptavidin with high sensitivity [16, 17]. It was also demonstrated that periodic arrays of Si nanoresonators can have sensitivities that are comparable to plasmonic nanostructure-based sensing systems [18]. Prostate-specific antigen (PSA) cancer marker in human serum was detected using array of Si discs with a limit of detection values of 0.69 ng/mL. Furthermore, there have been reports on the surface-enhanced spectroscopy based on all-dielectric nanoantennas [19–22]. The efficient coupling of high quantum yield emitters with dielectric fields has led to large enhancement factors comparable to plasmonic nanostructures. In spite of

✉ Sudhir Cherukulappurath
sudhir.c@unigoa.ac.in

[1] Physics Department, Goa University, Taleigao Plateau, Goa 403206, India

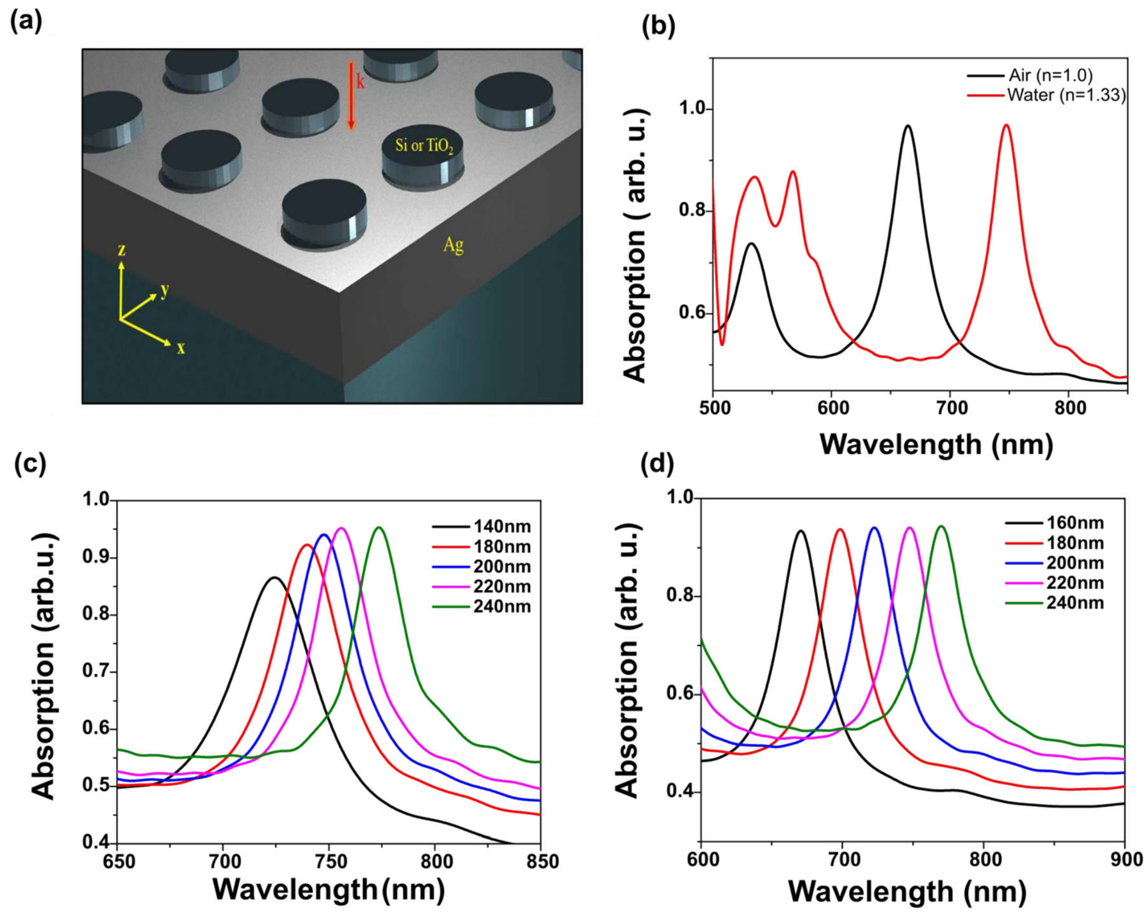

Fig. 1 **a** Schematic of the hybrid dielectric nanoparticle on a metal used for simulations. **b** Absorption spectrum of the dielectric nanoresonator arrays on silver with surrounding medium is air (black) and water (red). **c** Variation of the resonance wavelength with interparticle distance (edge to edge). The diameter of the particles is fixed at 220 nm. **d** Variation of resonance wavelength with particle diameter. Here the interparticle distance is fixed 200 nm

these emerging reports, dielectric nanoresonators are yet to replace plasmonic nanostructures in sensing applications mainly due to the fact that the local electromagnetic field enhancements in dielectric nanoresonators are poor compared to their plasmonic counterparts. Most of the electric and magnetic field hot-spots remain confined inside the dielectric medium. It is advantageous to have systems that can combine the properties of both the dielectric as well as plasmonic resonators. In particular, dielectric nanoparticles on metallic substrates have shown to exhibit coupled resonances.

In this letter, a hybrid photonic-plasmonic system is proposed for enhanced sensing applications. Several studies have shown that single dielectric resonator placed near a metallic film presents interesting optical behavior from the coupling of magnetic resonances of the dielectric to the metallic film [23–25]. While such hybrid systems have been reported, they have largely been restricted to the terahertz region [26–28] or infrared wavelengths [29]. Recently, Zou et al. demonstrated a nanoscale dielectric array-based plasmonic absorber system consisting of TiO_2 particles on silver film [30]. The authors showed that surface plasmon polariton (SPP) wave was excited by the coupling of magnetic resonances of the dielectric particles with the metallic film yielding a perfect absorbance of the incident light. However, there has been no report on the study of effect of parameters such as diameter of the dielectric resonators, distance between them, and their capabilities for sensing. Here, we report a theoretical simulation study of hybrid photonic-plasmonic subwavelength structures for sensing applications in the optical wavelengths.

A schematic of the proposed geometry is shown in Fig. 1a. An array of cylindrical high-refractive index particle (TiO_2) of height 50 nm are formed on metallic (Ag or Au) film. The metallic film is made sufficiently thick (200 nm) so that light is not transmitted through the film. The film may be supported by a glass or Si substrate in experiments. The diameter of the dielectric particle and the period of spacing between the particles are varied independently to tune the optical resonances. The particle array is excited using a normally incident plane polarized electromagnetic wave. Due to the symmetry of the structures, the reflection spectra are polarization independent. The far-field reflected light is monitored and the absorption spectrum is deduced. The magnetic and as electric resonances of the dielectric subwavelength

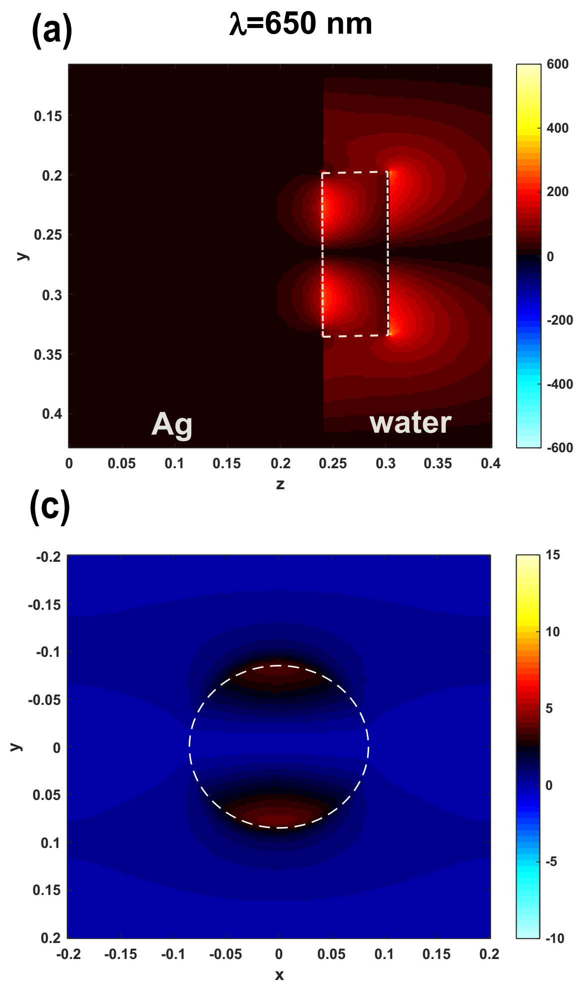

Fig. 2 **a** Electric field plot along the z-direction for the dielectric particle on metal film for an incident wavelength of **a** 650 nm and **b** 700 nm. The incident light is a plane wave polarized along the y-axis. **c**, **d** The corresponding electric field plots for the x-y plane 5 nm above the dielectric nanoresonator

particles couple with the SPP on the metal film substrate under right conditions. The refractive index of the medium that surrounds the dielectric nanoparticles is varied and the shifts in the resonances are observed.

Results and Discussion

The simulations were carried out using a FDTD-based software (Optiwave). Due to computational limitations in simulations, the grid spacing was kept at 5 nm for absorption spectra and 2 nm for electromagnetic field simulations. The typical absorption spectrum for the system is shown in Fig. 1b. Here, the particles have a diameter of 170 nm and the interparticle distance is 400 nm (center to center distance) with air (in black) and water (in red) as the surrounding media. A strong absorption peak around 650 nm and peaks corresponding to multipolar resonances can be observed in the absorption spectrum for air as surrounding medium. This is in agreement with that reported in ref. [31] with similar parameters. For water, the main resonance peak is red-shifted to 800 nm. In order to bring back the resonance wavelength to the visible range, the particle size and interparticle distances are appropriately chosen. The TiO_2 particles are considered as cylinders with height of 50 nm. The distance between neighboring particles is set to 400 nm. The absorbance plot is obtained from the reflection monitor placed in the far-field of the structure. For sensing applications, the strong peak arising due to collective resonances of the array of particles at the far-field is exploited. Due to the symmetry in the arrangement of particles, the resonance positions are independent of the polarization direction of the electric field. In order to demonstrate the tunability of resonances, the diameter and interparticle distances were varied independently. Figure 1c shows the effect of interparticle distance for a given diameter. The absorption spectrum with changing diameter while keeping the interparticle distance a constant is plotted in Fig. 1d. These simulation results demonstrate that it is possible to tune the resonance wavelengths in a similar fashion as for plasmonic nanoparticle arrays.

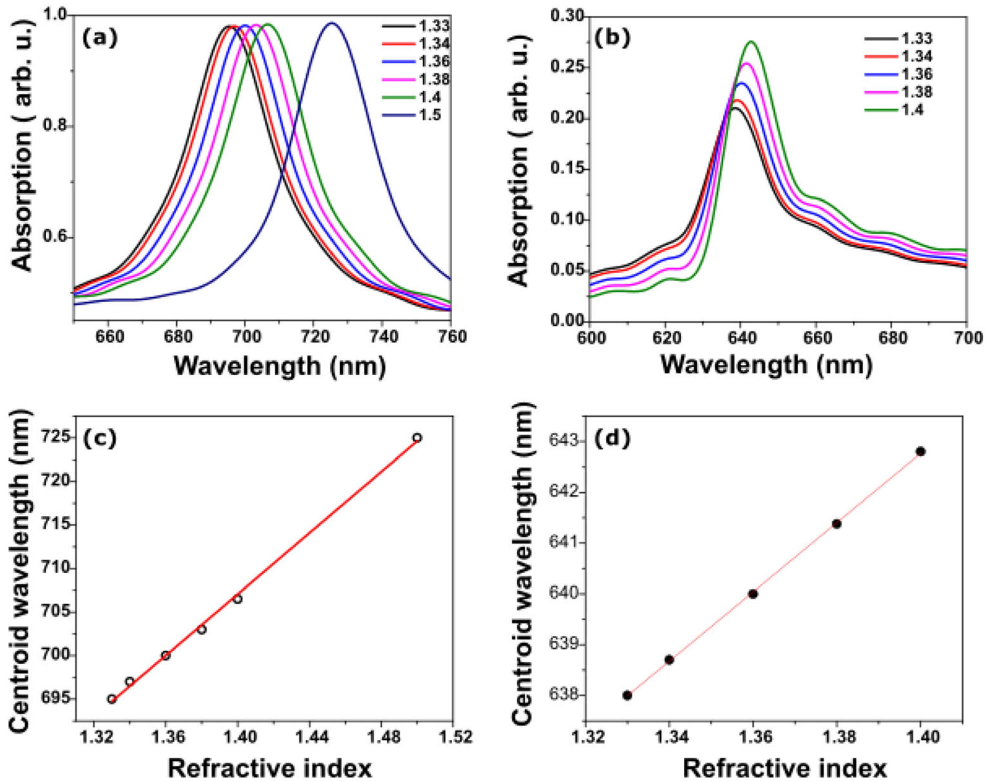

Fig. 3 Absorbance plots for TiO_2 resonator arrays on silver film (**a**) and on glass (**b**). The corresponding centroid wavelength versus refractive index of the surrounding medium is given in **c**, **d** respectively

In Fig. 2, the results of electric field simulations are shown. The time-averaged electric field along the propagation direction (E_z) for the TiO_2 nanoresonators on Ag film at an incident wavelength of 650 nm is given in Fig. 2a. The incident light is considered to be a plane wave polarized along the y-direction. It can be noted that at this non-resonant excitation, the local-field enhancement around the particle is weak. Electric field plot for an incident wavelength of 700 nm (near the resonance) is shown in Fig. 2b. A strong electric field enhancement around the dielectric resonator can be observed in this case. The corresponding near field distribution along the x-y direction at a distance of 5 nm from the nanoparticle is shown in Fig. 2c, d respectively. The strong local field enhancement along the y-direction around the nanoparticle at resonance wavelength of 700 nm can be observed.

In order to demonstrate bulk refractive index sensitivity (BRIS) of the device, the refractive index of the surrounding medium was varied from 1.33 to 1.5 in small steps. The TiO_2 particles are having a diameter of 170 nm and separated by 230 nm from each other (edge to edge). The corresponding shift in the absorption peak can be observed in Fig. 3a. For TiO_2 particles on glass, the shift in the peak wavelength of the absorption is shown in Fig. 3b. BRIS is often expressed in terms of the amount of shift in the centroid wavelength of the resonance to the change in refractive index

$$S = \frac{d\lambda_p}{dn} \tag{1}$$

where λ_p denotes the peak wavelength [3]. A plot of the centroid wavelength as a function of refractive index is

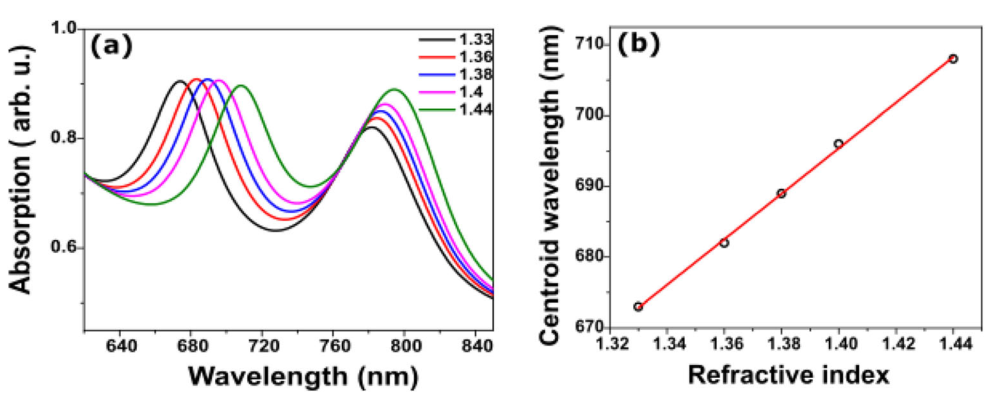

Fig. 4 **a** Absorption spectra of the Au–TiO_2 on Ag film with changing refractive index. **b** Peak wavelength shift versus refractive index for the peak 2 in (**a**). The red line is a linear fit the slope of which gives a sensitivity of 322 RIU/nm

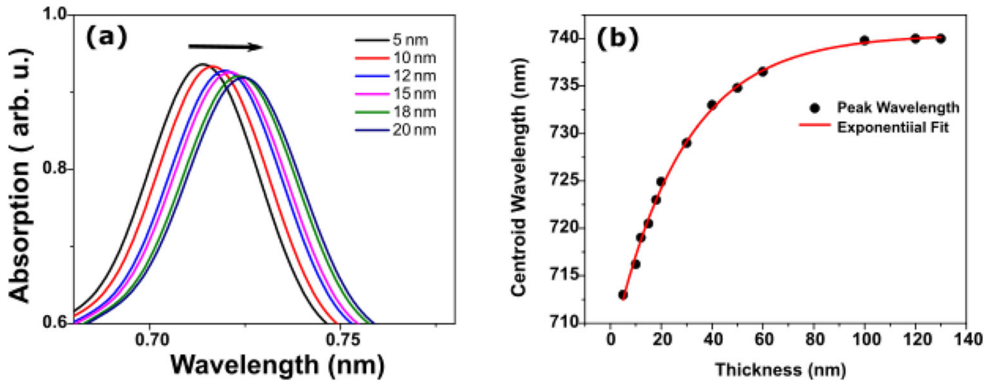

Fig. 5 **a** Absorbance plots for different thickness of layer of refractive index 1.45. The black arrow indicates the shift in the peak wavelength with increasing thickness. **b** Peak wavelength versus thickness of the layer. The red plot indicates an exponential fitting to the points

given in Fig. 3c. The slope of the linear fit to the points gives the BRIS of the device. In this case, the BRIS value for Ag–TiO_2 system is 176 nm/RIU. This value is comparable to the sensitivity of LSPR sensors that have been reported previously [3]. Figure 3d shows the BRIS plots for TiO_2 particles of same dimensions on glass substrate (without silver). It is observed that although the resonances have very small line widths as the losses related to plasmonic film are absent, the shift in resonance peak with refractive index is also very small. The refractive index sensitivity of TiO_2 on glass system is 68 nm/RIU (Fig. 3d) which is comparatively lower than the hybrid plasmonic photonic scheme. For refractive index sensing applications, it is not only the shift in the peak that is a measure of sensitivity but the line width of resonances is also an important factor in calculating the efficiency of the device. Peak broadening, predominantly due to multipolar resonance excitations and damping losses, can be significant in characterizing the sensing capabilities of nanoparticle-based devices. Figure of merit (FOM) of a device, obtained by dividing the sensitivity by line-width of the resonance is often considered to be a better measure of the sensor. It takes into account the shift in the resonance due to changes in refractive index as well as the inherent losses in the device, thereby allowing for a direct comparison between different sensing platforms.

$$\mathrm{FOM} = \frac{S}{\Delta\lambda} \tag{2}$$

In the case of Ag film–TiO_2 particle arrays, the FOM obtained is 4.9 which is higher than some of the LSPR sensing systems. Such good FOM value is achievable owing to the small linewidth (lower losses) of the dielectric resonators. We now consider a thin gold layer on the TiO_2 nanoparticles thereby making it like a hybrid metal-insulator-metal system. The addition of Au layer on the dielectric particles introduces new resonance peak in the visible region to the absorption spectrum as shown in Fig. 4a. The peak at the lower wavelength (centered around 672 nm for a refractive of 1.33) is attributed to the coupling of surface plasmons on the gold layer while the second peak (centered around 780 nm) is from the resonance of the dielectric particle coupled to the Ag film. This can be easily verified by performing the simulations with and without the top Au layer on the TiO_2 resonators. In Fig. 4b, the shift in the centroid wavelength with refractive index change is shown. The slope of the linear fit gives a sensitivity of 322 nm/RIU for such a device. This is much higher than the sensitivity values for TiO_2 on glass or TiO_2 on Ag film.

For biosensing applications, surface sensitivity is often considered more important than bulk sensitivity. Simulations to verify the surface-sensing capabilities of the hybrid photonic-plasmonic nanoresonators, layer of thickness from 10 to 100 nm of refractive index 1.45 was placed on the nanoparticles. The effect of layer thickness on the resonance wavelength is shown in Fig. 5a.

In the case of local refractive index sensing using plasmonic nanoparticles, the initial shifts appear linear but by addition of few more layers on the surface, the shift becomes smaller. This is due to the fact that local electromagnetic field of the plasmonic nanoparticle decay rapidly after few nanometers of distance from it. However, in the case of dielectric nanoresonators, decay of the local electromagnetic field is much slower with distance. The shift in resonance wavelength remains linear up to 30 nm of thickness and then slowly levels out (Fig. 5b). Hence, the device can be used for sensing thicker layers of molecules in comparison to LSPR sensing. Table 1 shows a comparison of the sensitivity and FOM of the configurations studied in this work. It can be observed that the TiO_2 particle arrays on glass gives a sensitivity of 68 nm/RIU with a FOM of 3.7 while TiO_2

Table 1 Comparison of sensitivity and FOM for different configurations

System	Peak λ (nm)	Δλ (nm)	Sensitivity S (nm/RIU)	FOM
TiO_2 on glass	640	18	68	3.7
Au on glass	690	135	264	2.0
TiO_2 on silver film	694	27	176	6.5
Au–TiO_2 on silver film	674	30	322	10.7

particle arrays on silver film shows a sensitivity of 176 nm/RIU with a FOM of 6.5. Adding a thin layer of gold to the TiO_2 nanoparticles on silver film further increases the sensitivity to 322 nm/RIU while the FOM obtained is as high a 10.5. These values are much larger than LSPR sensors [3]. For example, an array of gold nanocylinders of diameter 100 nm on glass shows a sensitivity of 264 with a FOM 2.0. The low FOM for plasmonic nanoparticles is mainly due to the broadening of the LSPR peaks due to absorption.

Conclusions

In conclusion, we have shown using simulations that hybrid plasmonic-photonic nanoparticle arrays can be used for refractive index sensing applications. In particular, we demonstrated that dielectric nanoparticle arrays on plasmonic metal film show large sensitivity for refractive index. Conventional LSPR-based sensing systems show large sensitivities but have lower FOM due to their broad resonances. These broad resonances are attributed to absorption losses inherent in the plasmonic metal. While dielectric particles have minimum optical losses thereby showing narrower resonances, the local field enhancement for dielectric nanoparticles are comparatively smaller. In this work, we have shown that by combining the two systems, it is possible to a sensing system with lower losses and narrower resonances thereby improving the sensitivity as well as obtaining higher FOM. For TiO_2 nanoresonator arrays on silver film, a sensitivity of 176 nm/RIU was obtained with a FOM of 6.5. Good wavelength tunability can be obtained for the nanoparticle arrays by varying either the size of the particles or by changing the interparticle distance. Both bulk as well as local refractive index sensing capabilities for the system were demonstrated. With the current advances in nanofabrication methods, it is possible to engineer and fabricate such hybrid devices on a large scale. High sensitivity and lower losses make the dielectric nanoparticle on plasmonic metal films a promising candidate for biosensing applications.

Acknowledgments The authors wish to acknowledge UGC-FRP (Faculty Recharge Programme) start up for partially funding the work.

Compliance with Ethical Standards

Conflict of Interest The authors declare that they have no conflict of interest.

References

1. Haes AJ, Van Duyne RP (2002) A nanoscale optical biosensor: sensitivity and selectivity of an approach based on the localized surface plasmon resonance spectroscopy of triangular silver nanoparticles. J Am Chem Soc 124:10596–10604
2. Willets KA, Van Duyne RP (2007) Localized surface plasmon resonance spectroscopy and SENSING. Annu Rev Phys Chem 58: 267–297
3. Mayer KM, Hafner JH (2011) Localized surface plasmon resonance sensors. Chem Rev 111:3828–3857
4. Evlyukhin AB, Novikov SM, Zywietz U, Eriksen RL, Reinhardt C, Bozhevolnyi SI, Chichkov BN (2012) Demonstration of magnetic dipole resonances of dielectric nanospheres in the visible region. Nano Lett 12:3749–3755
5. Zheludev NI, Kivshar YS (2012) From metamaterials to metadevices. Nat Mater 11:917–924
6. Zou L, Withayachumnankul W, Shah CM, Mitchell A, Bhaskaran M, Sriram S, Fumeaux C (2013) Dielectric resonator nanoantennas at visible frequencies. Opt Express 21:1344–1352
7. Kuznetsov AI, Miroshnichenko AE, Brongersma ML, Kivshar YS, Lukyanchuk B (2016) Optically resonant dielectric nanostructures. Science 354
8. Krasnok AE, Miroshnichenko AE, Belov PA, Kivshar YS (2013) All-dielectric nanoantennas. 8806
9. Krasnok A, Makarov S, Petrov M, Savelev R, Belov P, Kivshar Y (2015) Towards all-dielectric metamaterials and nanophotonics. 9502
10. Regmi R, Berthelot J, Winkler PM, Mivelle M, Proust J, Bedu F, Ozerov I, Begou T, Lumeau J, Rigneault H, García-Parajó MF, Bidault S, Wenger J, Bonod N (2016) All-dielectric silicon nanogap antennas to enhance the fluorescence of single molecules. Nano Lett 16:5143–5151
11. Ollanik AJ, Oguntoye IO, Hartfield GZ, Escarra MD (2019) Highly sensitive, affordable, and adaptable refractive index sensing with silicon-based dielectric metasurfaces. Adv Mater Technol 4: 1800567
12. Staude I, Pertsch T, Kivshar YS (2019) All-dielectric resonant meta-optics lightens up. ACS Photon 6:802–814
13. García-Etxarri A, Gómez-Medina R, Froufe-Pérez LS, López C, Chantada L, Scheffold F, Aizpurua J, Nieto-Vesperinas M, Sáenz JJ (2011) Strong magnetic response of submicron Silicon particles in the infrared. Opt Express 19:4815–4826
14. Groep J, Polman A (2013) Designing dielectric resonators on substrates: combining magnetic and electric resonances. Opt Express 21:26285–26302
15. Sautter J, Staude I, Decker M, Rusak E, Neshev DN, Brener I, Kivshar YS (2015) Active tuning of all-dielectric metasurfaces. ACS Nano 9:4308–4315
16. Yan J, Liu P, Lin Z, Yang G (2016) New type high-index dielectric nanosensors based on the scattering intensity shift. Nanoscale 8(11):5996–6007
17. Bontempi N, Chong KE, Orton HW, Staude I, Choi D-Y, Alessandri I, Kivshar YS, Neshev DN (2017) Highly sensitive biosensors based on all-dielectric nanoresonators. Nanoscale 9(15):4972–4980
18. Yavas O, Svedendahl M, Dobosz P, Sanz V, Quidant R (2017) On-a-chip biosensing based on all-dielectric nanoresonators. Nano Lett 17:4421–4426
19. Albella P, Poyli MA, Schmidt MK, Maier SA, Moreno F, Sáenz JJ, Aizpurua J (2013) Low-loss electric and magnetic field-enhanced spectroscopy with subwavelength silicon dimers. J Phys Chem C 117:13573–13584
20. Rodriguez I, Shi L, Lu X, Korgel BA, Alvarez-Puebla RA, Meseguer F (2014) Silicon nanoparticles as Raman scattering enhancers. Nanoscale 6(11):5666–5670
21. Bontempi N, Salmistraro M, Ferroni M, Depero LE, Alessandri I (2014) Probing the spatial extension of light trapping-induced enhanced Raman scattering in high-density Si nanowire arrays. Nanotechnology 25:465705

22. Cambiasso J, König M, Cortés E, Schlücker S, Maier S (2018) Surface-enhanced spectroscopies of a molecular monolayer in an all-dielectric nanoantenna. ACS Photon 5:2
23. Li L, Hutter T, Finnemore AS, Huang FM, Baumberg JJ, Elliott SR, Steiner U, Mahajan S (2012) Metal oxide nanoparticle mediated enhanced Raman scattering and its use in direct monitoring of interfacial chemical reactions. Nano Lett 12:4242–4246
24. Huang Z, Wang J, Liu Z, Xu G, Fan Y, Zhong H, Cao B, Wang C, Xu K (2015) Strong-field-enhanced spectroscopy in silicon nanoparticle electric and magnetic dipole resonance near a metal surface. J Phys Chem C 119:28127–28135
25. Li H, Xu Y, Xiang J, Li XF, Zhang CY, Tie SL, Lan S (2016) Exploiting the interaction between a semiconductor nanosphere and a thin metal film for nanoscale plasmonic devices. Nanoscale 8(45):18963–18971
26. Headland D, Nirantar S, Withayachumnankul W, Gutruf P, Abbott D, Bhaskaran M, Fumeaux C, Sriram S (2015) Terahertz magnetic mirror realized with dielectric resonator antennas. Adv Mater 27:7137–7144
27. Lee WSL, Kaltenecker K, Nirantar S, Withayachumnankul W, Walther M, Bhaskaran M, Fischer BM, Sriram S, Fumeaux C (2017) Terahertz near-field imaging of dielectric resonators. Opt Express 25:3756–3764
28. Headland D, Monnai Y, Abbott D, Fumeaux C, Withayachumnankul W (2018) Tutorial: terahertz beamforming, from concepts to realizations. APL Photon 3:051101
29. Malheiros-Silveira GN, Hernandez-Figueroa HE (2015) Dielectric resonator nanoantenna coupled to metallic coplanar waveguide. IEEE Photon J 7:1–7
30. Zou C, Gutruf P, Withayachumnankul W, Zou L, Bhaskaran M, Sriram S, Fumeaux C (2016) Nanoscale TiO2 dielectric resonator absorbers. Opt Lett 41:3391–3394